Isothermal CO_2 Separation Enabled by Redox-active Mixed Oxide Sorbents

Mahe Rukh[‡], *Runxia Cai*[‡], *Leo Brody*, *Fanxing Li**

Department of Chemical and Biomolecular Engineering, North Carolina State University, 911 Partners Way, Raleigh, North Carolina 27695-7905, USA

[‡] *These authors contributed equally to this work*

**Corresponding author, fli5@ncsu.edu*

Abstract

This study reports an isothermal CO_2 capture strategy using redox-active perovskite oxides and demonstrates its application in sorption-enhanced hydrogen production. Using a thermodynamic analysis, we investigated the relationship between the equilibrium oxygen partial pressure and the extent of CO_2 sorption as well as the theoretical hydrogen purity. To validate the concept, calcium and cobalt co-doped $SrFeO_3$ ($Sr_{1-x}Ca_xFe_{1-y}Co_yO_{3-\delta}$) samples were screened experimentally to assess their (isothermal) CO_2 sorption capacity and reducibility. The optimal sorbent, $Sr_{0.6}Ca_{0.4}Fe_{0.7}Co_{0.3}O_{3-\delta}$ (SCFC-6473), underwent further characterizations and was used for isothermal sorption-enhanced steam reforming (iSESR) of glycerol to produce H_2, achieving 93 vol% H_2 purity. In addition, we present iSESR of biogas and isothermal sorption-enhanced gasification (iSEG) of pulverized pine by $Sr_{0.875}Ba_{0.125}MnO_{3-\delta}$ (SBM 718) to validate the generalizability of the proposed concept for a variety of applications. Nearly 90% syngas efficiency was demonstrated for iSEG of biomass while producing a hydrogen enriched (73 vol.%) syngas product.

23 **TOC**

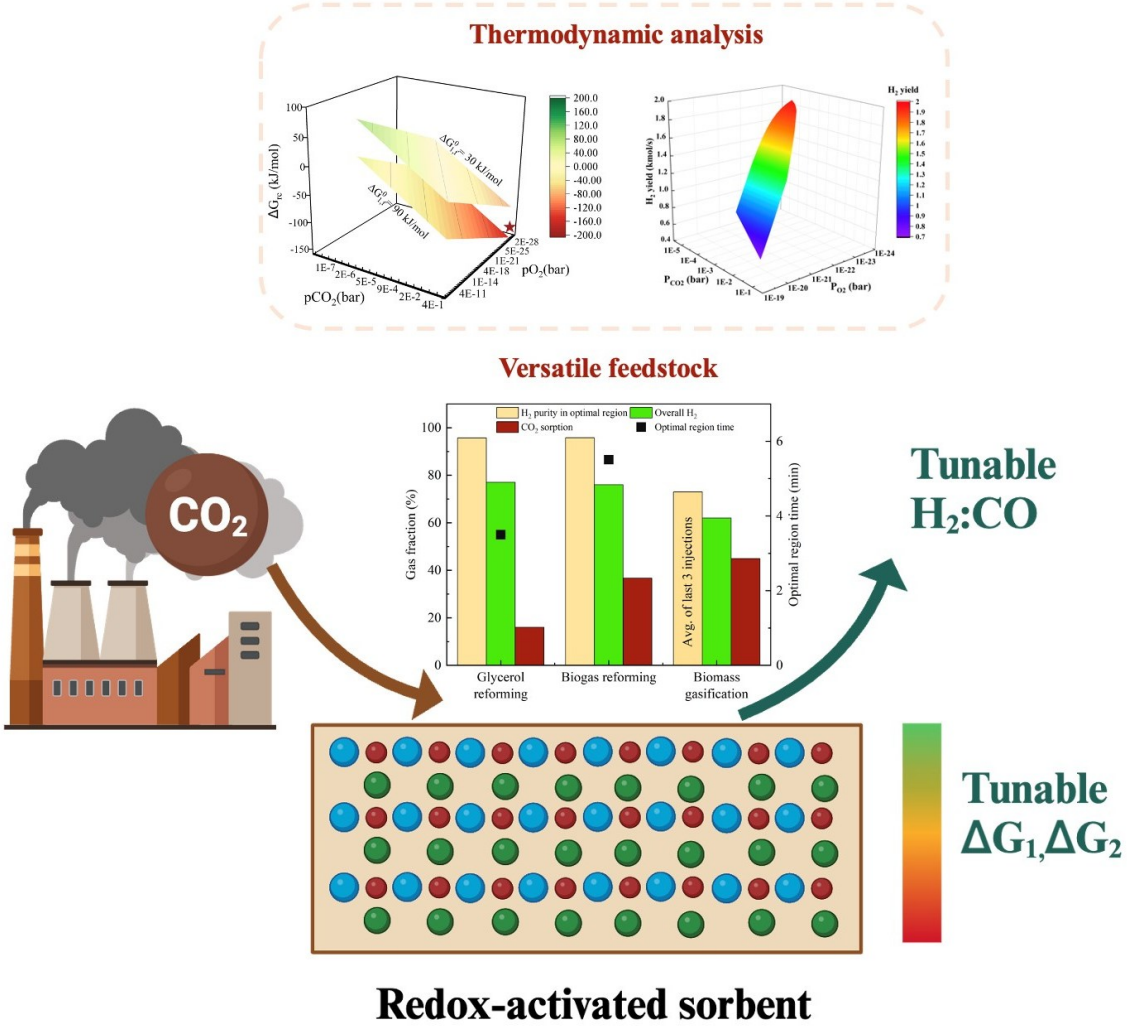

24

25

26

27

28

1.0 Introduction

CO_2 emissions have almost tripled since 1960, primarily driven by fossil fuel combustion and industrial processes.[1] Renewable energy sources such as solar, wind, and biomass are the ultimate solution towards a low-carbon society.[2,3] However, they still face challenges for widespread adoption. For instance, wind and solar energy are largely limited to power generation and confront challenges related to intermittency, which can hinder their integration into wide-area synchronous grids.[4] Biomass, on the other hand, provides a renewable carbon source for energy, fuel, and chemical production. However, state-of-the-art approaches for biomass conversion, such as gasification and pyrolysis, face challenges in terms of complexity, efficiency, and economic viability.[5,6] Therefore, there is a growing demand for intensified processes that can efficiently convert biomass into hydrogen or hydrogen-enriched syngas. One promising approach is sorption-enhanced reforming or gasification of biomass and biomass derivatives, which involves the thermochemical conversion of the carbonaceous feedstock in the presence of a CO_2 sorbent at high temperatures. However, the main challenge resides in severe limitations in sorbent performance, since most sorbents require a significant temperature swing during the endothermic sorbent regeneration step and are prone to deactivation.[7–11] The same limitations also apply to sorbent-based CO_2 capture technologies in the context of carbon capture and sequestration in fossil fuel conversion.[12–19]

All sorbent-based CO_2 capture methods require a regeneration or decarbonation step aside from carbon mineralization, which aims to permanently store CO_2 as stable carbonates. Although a decrease in CO_2 pressure by vacuuming could, in theory, drive the decarbonation reaction, vacuuming alone is usually unable to provide a sufficient driving force for regeneration due to the strong sorbent-CO_2 interactions. Moreover, achieving and maintaining low vacuum conditions (e.g.

below 5 kPa) at large scale is a significant cost challenge.[20,21] For practical usage of high-temperature sorbents for thermochemical biomass conversion (> 500 ºC), a substantial temperature increase is required to achieve efficient regeneration of sorbents.[7,8,11,22,23] The large temperature swing and strong endothermicity of the decarbonation step lead to a high energy and economic penalty.[10,24–26] Therefore, a CO_2-sorbent that can operate isothermally would greatly simplify the reactor system design and improve the process efficiency. Unfortunately, existing high-temperature sorbents, such as CaO or modified CaO,[13,27–39] and mixed alkali oxide and alkaline-earth oxide [24,40–50], all typically require a large temperature increase (> 100 ºC) in the context of sorption-enhanced biomass gasification.[51–53] Moreover, they tend to deactivate under repeated carbonation-decarbonation cycles, unless an energy-intensive sorbent re-activation step is implemented.[54,55]

This study presents and validates a unique approach to design a new class of sorbent materials capable of isothermal operation with excellent cyclic stability. This is accomplished by carefully choosing redox-active mixed oxides that are responsive not only to shifts in external CO_2 partial pressure (p_{CO_2}) but also to variations in the oxygen partial pressure (p_{O_2}). The redox-active component, which induces carbonation under a reducing (low p_{O_2}) environment and decarbonation under an oxidizing (high p_{O_2}) environment, introduces a new dimension in sorbent design and operation. This enables their efficient utilization, especially in the realm of carbon-free hydrogen production from biogenic feedstocks. Specifically, we first present a thermodynamic analysis framework to establish the feasibility of the proposed sorbent design strategy and to facilitate the rational selection of suitable sorbent materials. The performance of these sorbents, e.g. $Sr_xCa_{1-x}Fe_yCo_{1-y}O_{3-\delta}$ (SCFC), $Sr_xBa_{1-x}Fe_yMn_{1-y}O_{3-\delta}$ (SBM) was subsequently validated

74 experimentally. We initially tested the SCFC materials using TGA on eight different samples.
75 Following this, SCFC 6482 was examined with *in-situ* XRD to investigate the dynamic phase
76 transitions. Subsequently, we tested SCFC 6473 for sorption-enhanced glycerol reforming in a
77 fixed bed configuration. Lastly, SBM 718 was evaluated for both sorption-enhanced biogas
78 reforming and biomass gasification to demonstrate the versatility of isothermal sorption
79 enhancement across various feedstocks.

80 As illustrated in Fig. 1, the isothermal CO_2 capture strategy utilizes two reactors with varying
81 oxygen partial pressure (p_{O_2}). In the first step, during the conversion of a carbonaceous fuel such
82 as biomass, reducing gases such as H_2, CO, and/or CH_4 are generated, creating a low p_{O_2}
83 environment. The redox-active mixed metal oxides are accordingly reduced, freeing up the highly
84 basic A-site cations such as Sr^{2+} to capture CO_2. The degree to which the sorbents are carbonated
85 is largely determined by the extent of metal oxide reduction under the reducing environment. In
86 the sequential regeneration under a high p_{O_2} environment, the carbonated sorbent and reduced
87 metal oxides will be contacted with air or O_2 to restore the mixed metal oxide phase, releasing the
88 CO_2. Integration of redox reactions with CO_2 absorption/desorption can also tailor the heat
89 distributions between the two reaction steps, enhancing the process efficiency. Coupling the
90 carbonation and decarbonation reactions with the external redox environment also creates an
91 additional dimension in tailoring the sorbent's operating window and performance by adjusting its
92 cation composition and redox properties, as elaborated below.

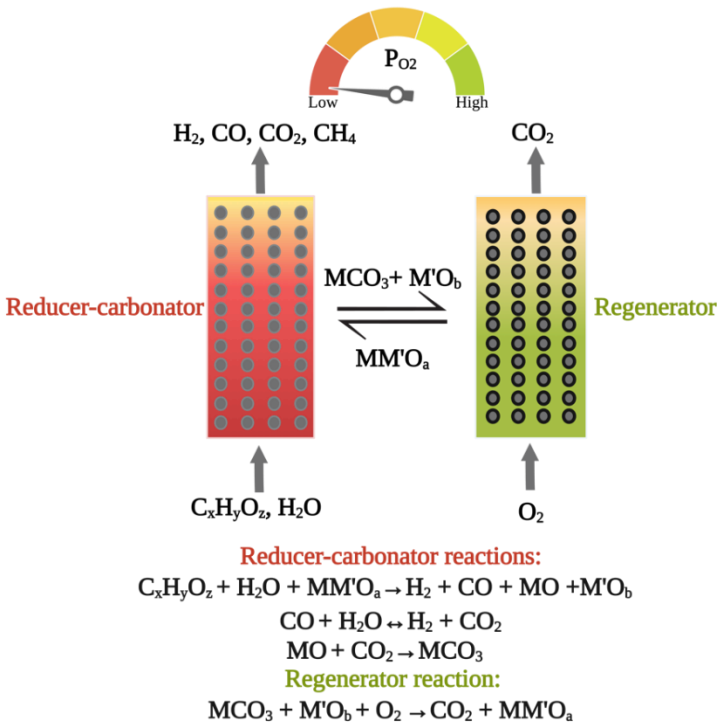

Fig. 1 Schematic diagram of the isothermal redox-active sorbent looping CO_2 capture scheme. $MM'O_a$ represents a generic mixed oxide sorbent.

2.0 Thermodynamic analysis approach

The thermodynamic analysis began with the effects of oxygen chemical potential (or equivalently oxygen partial pressure) on the thermodynamic feasibility of CO_2 absorption. $Sr_xCa_{1-x}Fe_yCo_{1-y}O_{2.5}$ and $Sr_xBa_{1-x}Fe_yMn_{1-y}O_{2.5}$ were selected as examples of redox-active CO_2 sorbents. Herein, x denotes the Sr molar fraction in the A-site, and y represents the Fe molar fraction in the B-site. For example, a simplified reaction scheme of CO_2 sorption by $Sr_{0.5}Ca_{0.5}Fe_yCo_{1-y}O_{2.5}$ involve Reactions 1-3. Under a reducing, low p_{O_2} environment, the B-site cation in the perovskite or brownmillerite phase is reduced, "freeing up" the highly basic A-site oxide (Reaction 1). The A-site oxide would then react with CO_2 to form carbonates (Reaction 2 and 3). The low p_{O_2} environment is consistent

103 with typical gasification or reforming conditions, which produces reducing gases such as H_2 and
104 CO.

$$Sr_{0.5}Ca_{0.5}Fe_yCo_{1-y}O_{2.5} \leftrightarrow 0.5\ SrO + 0.5\ CaO + y\ FeO + (1-y)\ CoO + 0.25\ O_2(g) \quad (1)$$

$$SrO + CO_2(g) \leftrightarrow SrCO_3 \quad (2)$$

$$CaO + CO_2(g) \leftrightarrow CaCO_3 \quad (3)$$

105 For single-phase sorbent undergoing an isothermal process, the change in chemical potential is
106 equivalent to the change in Gibbs free energy (ΔG), and the standard pressure of the gaseous
107 species is set to unity. The fugacity of a component in an ideal gas mixture is equal to its partial
108 pressure P_j. Hence, the Gibbs free energies of Reactions 1-3 can be described by Eqs. (4-6)

$$\Delta G_{1,c} = \Delta G^0_{1,f} + RT \ln p^{0.25}_{O_2} \quad (4)$$

$$\Delta G_{2,c} = \Delta G^0_{2,f} + RT \ln p^{-1}_{CO_2} \quad (5)$$

$$\Delta G_{3,c} = \Delta G^0_{3,f} + RT \ln p^{-1}_{CO_2} \quad (6)$$

109 The overall Gibbs free energies combining Reactions 1-3 can be described by Eq. (7).

$$\Delta G_{rc} = \Delta G_{1,f} + 0.5\left(\Delta G_{2,f} + \Delta G_{3,f}\right) \quad (7)$$

110 Reactions 1-3 are reversed when the redox-active CO_2 sorbent is decarbonated and regenerated,
111 so the change in the overall Gibbs energy during the regeneration step (ΔG_{re}) can be described
112 by Eq. (11) after combining Eqs. 8-10.

$$\Delta G_{1,r} = -\Delta G_{1,f}^{0} + RT \ln p_{O_2}^{-0.25} \quad (8)$$

$$\Delta G_{2,r} = -\Delta G_{2,f}^{0} + RT \ln p_{CO_2} \quad (9)$$

$$\Delta G_{3,r} = -\Delta G_{3,f}^{0} + RT \ln p_{CO_2} \quad (10)$$

113 A negative ΔG_{rc} for a given perovskite sorbent indicates thermodynamic favorability of
114 reduction-carbonation under a specific O_2 partial pressure, p_{O_2}, and CO_2 partial pressure, p_{CO_2}.
115 Likewise, a negative ΔG_{re} indicates a thermodynamic favorability of decarbonation.

$$\Delta G_{re} = \Delta G_{1,r} + 0.5\left(\Delta G_{2,r} + \Delta G_{3,r}\right) \quad (11)$$

116 Furthermore, in the context of sorption-enhanced hydrogen production, the most abundant
117 component in the gas phase, i.e., hydrogen and steam, can be utilized to estimate the oxygen partial
118 pressure of the system. In this case, the oxygen partial pressure is correlated with $\frac{p_{H_2}}{p_{H_2O}}$, which
119 can be described by Reaction (12). Therefore, both ΔG_{rc} and ΔG_{re} are the functions of $\Delta G_{1,f}^{0}$,
120 $\frac{p_{H_2}}{p_{H_2O}}$ and p_{CO_2}. To assess the thermodynamic favorability of carbonation and regeneration steps,
121 the following ranges were considered: standard formation energy of the perovskite oxide $\Delta G_{1,f}^{0}$
122 =30~90 kJ/mol (the range was roughly estimated based on the DFT calculation), $\Delta G_{1,f}^{0}$,
123 $p_{CO_2} = 0.00001 - 0.9$ bar. During the regeneration step, $\frac{p_{H_2}}{p_{H_2O}}$ was varied between 1^{-10} to 1 which

corresponded to the following p_{O_2} range: 0.99~2^{-20} bar. We varied the p_{H_2} and p_{H_2O} ratio to cover a realistic range of reactor conditions for the SESR process.[56]

$$2H_2(g) + O_2(g) \leftrightarrow 2H_2O(g) \quad (12)$$

Given the vast material design space for redox activated sorbents, the presented thermodynamic framework is useful as a first pass for narrowing down suitable candidate materials (without considering kinetic and transport effects). Sorbent design and operation principles for the isothermal process are briefly discussed in this section. The isothermal sorption-enhancement approach incorporates oxygen partial pressure as an additional design variable, enabling a more precise prediction of favorable phase transition conditions. We initiate our investigation by exploring the impacts on process variables, namely (i) perovskite composition, (ii) p_{O_2}, and (iii) p_{CO_2}, on the thermodynamic favorability of using $Sr_{0.5}Ca_{0.5}Fe_yCo_{1-y}O_{2.5}$ and $Sr_{0.5}Ba_{0.5}Fe_yMn_{1-y}O_{2.5}$ perovskite oxides for sorption-enhancement. Fig. 2a and 2c illustrate the dependence of reduction-carbonation and regeneration-decarbonation ΔG on the gas environment using the former composition, and Fig. 2b and 2d display the relationship for the latter. The two planes in each figure represent ΔG of a specific composition of sorbent with a fixed $\Delta G^0_{1,f}$ of 30 or 90 kJ/mol. Additionally, the equilibrium composition analysis was conducted using Aspen Plus simulation software. A detailed description of the methodology used for this analysis can be found in the supplementary file.

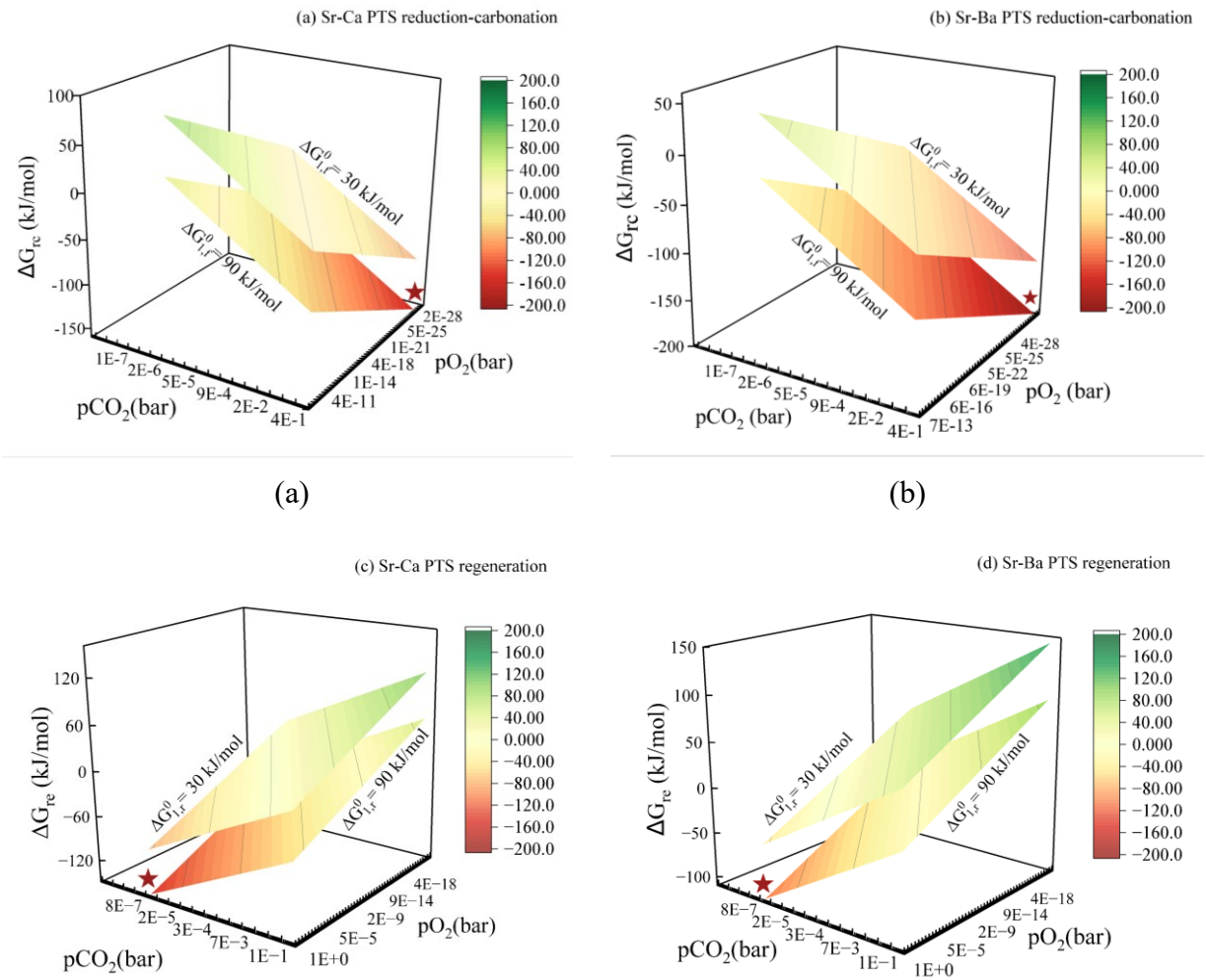

Fig. 2 Overall Gibbs free energy change in the *carbonation step* as a function of $\Delta G^0_{1,f}$, p_{O_2}, and p_{CO_2} for (a) $Sr_{0.5}Ca_{0.5}Fe_yCo_{1-y}O_{2.5}$ (b) $Sr_{0.5}Ba_{0.5}Fe_yMn_{1-y}O_{2.5}$; and overall Gibbs free energy change in the *regeneration step* as a function of $\Delta G^0_{1,r}$, p_{O_2}, and p_{CO_2} for (c) $Sr_{0.5}Ca_{0.5}Fe_yCo_{1-y}O_{2.5}$ (d) $Sr_{0.5}Ba_{0.5}Fe_yMn_{1-y}O_{2.5}$ (T=750 ºC and P_{total}=1 atm). The highly favorable region is marked with a star symbol.

142

3.0 Results and Discussion

3.1 Thermodynamic analysis

As shown in Figs. 2a and 2b, the carbonation reaction is favored by an increase in CO_2 partial pressure and/or a decrease in O_2 partial pressure, as reflected by a more negative ΔG_{rc} under such conditions. This feature is distinct from that of conventional sorbents which responds solely to CO_2 partial pressure change. This increased flexibility, i.e., response of the carbonation reaction to p_{O_2}, enhances the tunability of the carbonation process compared to traditional sorbents. By reducing the O_2 partial pressure, the carbonation reaction can be favorable even at low CO_2 concentrations, ensuring a high hydrogen purity. The equilibrium CO_2 pressure of $BaCO_3$ at 750 ^oC (0.0036 bar) is much lower than that of $CaCO_3$ (0.26 bar). Therefore, carbonation is more thermodynamically favorable when the A site incorporates Ba instead of Ca.

Opposite to the carbonation step, the regeneration step is favored under decreased CO_2 partial pressure and increased O_2 partial pressure (Figs. 2c/d). Regenerating the Ba-doped perovskites is more difficult than for the Ca-doped perovskites, requiring lower CO_2 concentrations and higher O_2 concentrations. Therefore, identifying the appropriate compositions of perovskite for the isothermal operation requires a careful balance of both the carbonation and regeneration steps. Beyond the two sorbents considered here, this simple and generalized approach can be used to assess the thermodynamic feasibility of other redox-active sorbents for the sorption-enhanced processes.

The H_2 yield and H_2 purity, predicted from equilibrium composition analysis for a carbon (char) gasification process, are illustrated in Fig. 3. The details of the equilibrium analysis are presented

in the SI file. Within the $p_{O_2,eq}$ range considered, C was fully gasified into syngas (H_2 and CO). Resulting from effective capture of CO_2, a maximum H_2 yield of 1.96 mol/mol C can be achieved at $p_{O_2,eq}$ of 1.49×10^{-23} bar and $P_{CO2,eq}$ of 2.24×10^{-4} bar. This H_2 yield is close to the theoretical maximum of 2 mol/mol C. Meanwhile, the H_2 purity is 99.2 vol %. The H_2 yield gradually declined with increasing $p_{O_2,eq}$ due to (partial) combustion of the produced H_2, which can balance the heat requirement for the gasification process. On the other hand, increased CO_2 removal by the sorbent, e.g. higher A-site basicity and/or higher B-site reducibility, can increase H_2 purity, and vice versa. Therefore, adjusting the $p_{O_2,eq}$ and $P_{CO2,eq}$ of the sorbent by tuning its compositions can vary the maximum H_2 yield and purity in the isothermal gasification process. This versatility makes it feasible to produce hydrogen enriched syngas product for various applications such as hydrogen production, Fischer-Tropsch synthesis, methanol production, or methanation reaction.

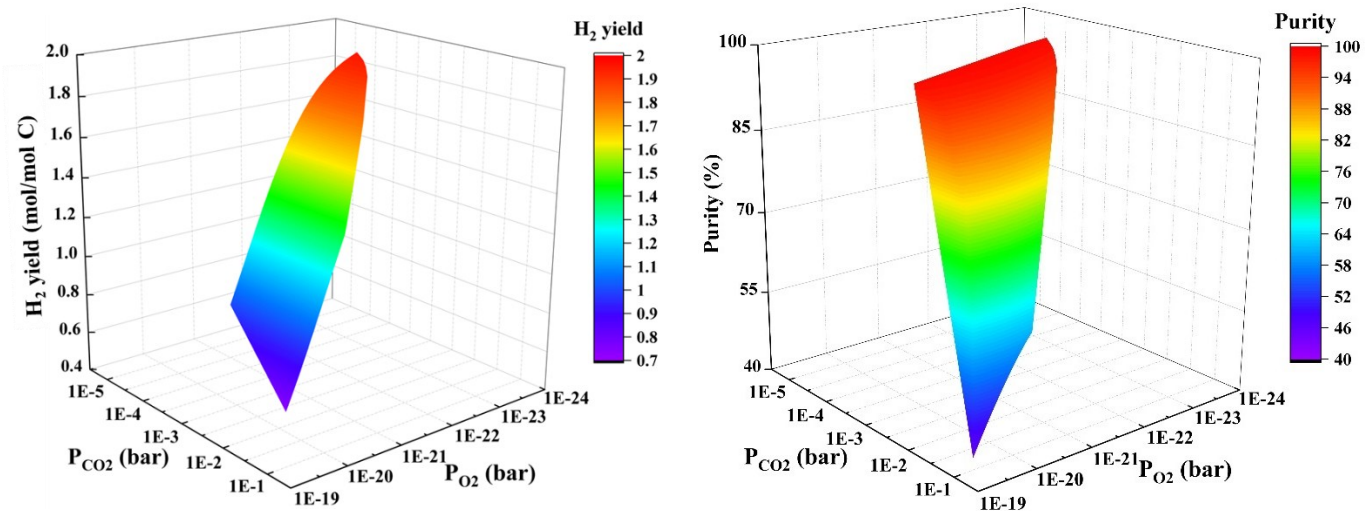

(a) (b)

Fig. 3 The impact of $p_{CO_2,eq}$, $p_{O_2,eq}$ on the (a) theoretical H_2 yield and (b) H_2 purity.

176

177 ## 3.2 Thermogravimetric analysis

178 The feasibility of isothermal CO_2 separation was first validated in a TGA using SCFC perovskite
179 oxides. **Fig. 4** summarizes the CO_2 sorption capacity and the reduction degree of the 8 screened
180 samples. These materials all demonstrated isothermal CO_2 capture at 750 °C. In general, the
181 sorption capacities correlate well with the degree of reduction, confirming our sorbent design
182 strategy. Particularly, SCFC 7382 demonstrated the highest sorption capacity and reduction degree
183 among the samples belonging to the SCFC x(1-x)82 group, while SCFC 6455 exhibited the best
184 performance in the SCFC 64y(1-y) groups. The presence of greater than 70% Sr in the A-site
185 resulted in a decrease in CO_2 sorption but a notable increase in degree of reduction, likely due to
186 the less favorable regeneration of $SrCO_3$ at 750 °C. For SCFC 64y(1-y) group, on the other hand,
187 as the molar amount of cobalt in the A-site increased from 10% to 50%, both sorption capacity
188 and reduction degree increased due to the enhanced reduction rate.[57] When Co doping exceeded
189 50%, both sorption capacity and reduction degree decreased, highlighting the importance of of
190 balancing the B-site cation compositions and reducibility.

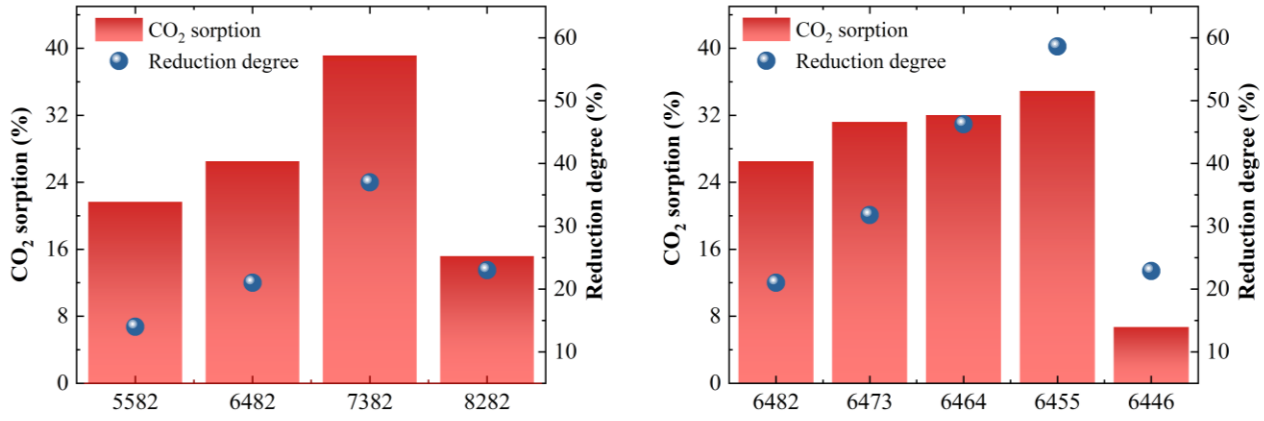

(a) (b)

Fig. 4 Comparisons of CO_2 sorption capacity and reduction degree among eight SCFC samples

191

192 ## 3.3 Phase transition behavior under in-situ XRD

193 The phase transition behaviors of the sorbents were also confirmed using *in-situ* XRD. As
194 illustrated in Fig. 5, *in-situ* XRD confirmed the phase reversibility of the perovskite sorbent during
195 isothermal operation. Initially, SCFC-6482 underwent a complete cycle of carbonation and
196 regeneration for pre-treatment. Subsequently, the samples were subjected to a series of different
197 gas atmospheres. The Fe_3O_4 peak first appeared at the beginning of the CO_2 region. The gradual
198 intensification of the Fe_3O_4 peak at ~35˚ confirmed the reduction of perovskite oxide to the B-site
199 metal oxides. Cobalt oxide peaks were ambiguous, likely attributed to the low doping amount of
200 cobalt in this sample. The diffraction pattern of the sample showed a visible increase in peak
201 intensity around $2\theta = 24.91^\circ$ and 25.58°, which slightly shifted from the characteristic peaks of pure
202 $SrCO_3$ at room temperature ($2\theta = 25.17^\circ$ and 25.8°). In addition, $CaCO_3$ peak briefly appeared at
203 ~28˚ in the CO_2-only region. It was swiftly decomposed to CaO ($2\theta = 36.25^\circ$) and remained visible

throughout the co-feeding stage. Importantly, the *in-situ* XRD results revealed the synergistic effect of H_2 and CO_2. Compared to co-feeding of H_2 and CO_2, feeding H_2 alone only resulted in a weak Fe_3O_4 peak, indicating a slow reduction of the sorbents. This observation is consistent with the results of the thermodynamic analysis, which shows the synergistic effects of p_{O_2} and p_{CO_2}.

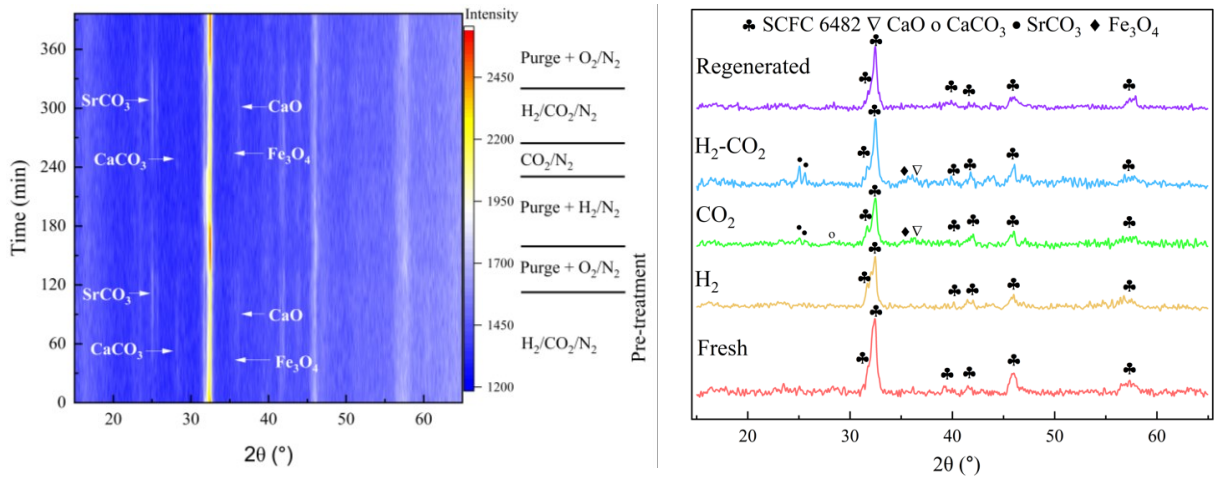

Fig. 5 (a) *In-situ* XRD diffraction pattern contour plots of SCFC-6482 under 750ºC (b) *In-situ* XRD patterns of fresh, reduced, and regenerated stages for co-feed and single-feed streams.

3.4 Isothermal sorption-enhanced reforming and gasification experiment

In a packed bed reactor, the SCFC 6473 sorbent demonstrated effective isothermal sorption performance for glycerol reforming, utilizing commercial NiO/Al_2O_3 for catalytic activity. CO_2 production in the initial 3 minutes of each cycle, attributed to unselective glycerol oxidation due to reduction of $ABO_{2.5+\delta}$ to $ABO_{2.5}$, which was addressed with a pre-reduction step (5 vol% H_2, 20

mins) before each cycle, resulting in 7.53 vol% decrease in CO_2 generation. Successive sorbent saturation led to decreased syngas yield and increased CO_2 concentration. The optimal H_2 production region, defined by CO_x concentration below 4.5 vol%, lasted an average of 5 minutes across 14 cycles, with a stable sorption capacity of approximately 16%. Analysis of reaction profile from mass spectrometry confirmed sorbent efficacy, exhibiting concentrated hydrogen during reforming and a notable CO_2 peak during regeneration (Fig. S3(a)). H_2 purity, particularly during the optimal region, consistently reached around 93 vol%, averaging approximately 76 vol% overall.

In addition to glycerol reforming, SBM 718, a Ba-containing sorbent, was tested for isothermal sorption-enhanced steam reforming of biogas at 850°C and S/C=2. During initial reforming period, CO_2 release occurred due to gradual reduction of $Sr_{0.875}Ba_{0.125}MnO_{3-\delta}$ to $Sr_{0.875}Ba_{0.125}MnO_{2.5}$ (Fig. S4(b)). Further reduction led to SrO and BaO formation, capturing CO_2 and favoring H_2 production. Similarly to glycerol reforming experiment, a sequential regeneration released significant CO_2, validating sorbent efficacy for isothermal sorption-enhanced hydrogen production. Gas concentrations remained consistent over 14 cycles, with an average overall H_2 concentration of ~78% and CO_2 under 10 vol%. The average sorption capacity observed is 36.65%, with the optimal H_2 production region lasting ~5.45 minutes where H_2 concentration averaged at ~96%. Furthermore, minimal deactivation was observed indicating sorbent durability.

The efficacy of SBM 718 in sorption-enhanced gasification of biomass (SEBG) was also evaluated in a laboratory-scale bubbling fluidized bed reactor at 850°C (Fig. S5). Fig. S6 (a) and (b) illustrate the gas compositions during the gasification step with five pulse injections of biomass. The 1st injection primarily resulted in significant CO_2 release with minimal H_2 production. However, H_2 gradually increased with each subsequent injection, peaking at an average of 73% in the last three

injections, while CO_2 fraction diminished to 11%. The high valent state of Mn cation in the 1st injection led to significant CO_2 release, but the subsequent reduction led to SrO and BaO formation, effectively capturing CO_2 and favoring water-gas-shift for H_2 generation. During the regeneration, substantial CO_2 release corresponded to approximately 45% sorption capacity, affirming the robustness of redox-active perovskite oxides for isothermal sorption-enhanced processes. Furthermore, estimated high heating value (HHV) efficiencies stand at 75% and 91% based on 5 and the last 4 injections, respectively. Correspondingly, low heating value (LHV) efficiencies for the same sets of injections are 73% and 88%, indicating enhanced energy conversion efficiency of the proposed system.

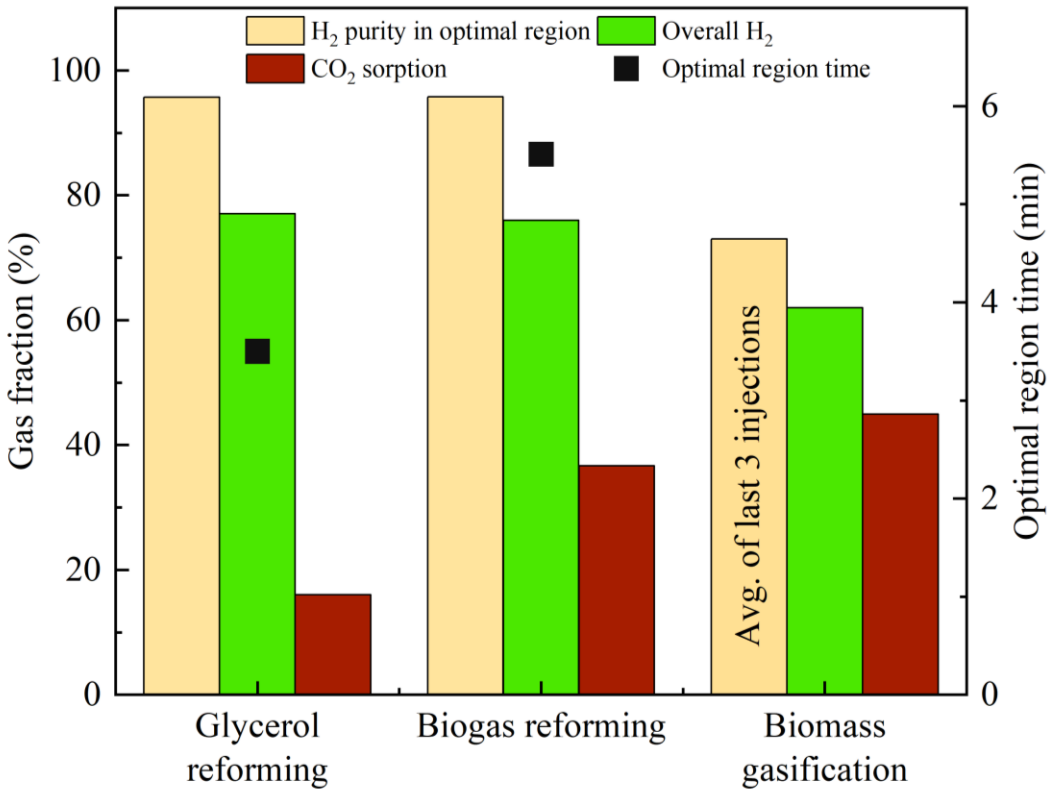

Fig. 6 Summary of isothermal sorption-enhanced glycerol reforming, biogas reforming and biomass gasification experimental results.

4.0 Conclusion

In summary, this study reports theoretical analysis and experimental validation of a unique family of redox-activated sorbents for isothermal sorption-enhanced reforming and gasification. Hydrogen and hydrogen enriched syngas was produced from a variety of biogenic feedstocks, showing a ~90% syngas generation efficiency from woody biomass with up to 73% H_2 concentration in the gasification product. Sorbents with various compositions, supported by thermodynamic analysis, showed excellent isothermal performance and cyclic stability. The isothermal approach, which also facilities autothermal operation through the redox-reactions of the B-site transition metal in the sorbent, offer distinct advantages compared to conventional sorbents in terms of energy efficiency, cyclic stability, tunability, and versatility in handling various biogenic feedstocks.

Supporting information

Thermodynamic analysis, Aspen simulation flowsheet, material synthesis, XRD, experimental procedure, and calculation methods.

Acknowledgements

This work was supported by the U.S. Department of Energy Office of Energy Efficiency & Renewable Energy (no. EE0008809) and the US National Science Foundation (CBET-1923468). The authors would like to acknowledge Prof. Stephen Kelley and Mr. Andrew Jones for providing and characterizing the woody biomass samples. We also acknowledge the use of the Analytical Instrumentation Facility (AIF) at the North Carolina State University, which is supported by the State of North Carolina and the National Science Foundation.

References

[1] NOAA climate.gov, Climate change and atmospheric Carbon Dioxide, https://www.climate.gov/news-features/understanding-climate/climate-change-atmospheric-carbon-dioxide#:~:text=Since%20the%20middle%20of%20the,the%20Global%20Carbon%20Budget%202023, (accessed May 21, 2024)

[2] S. Bilgen, K. Kaygusuz, A. Sari, Renewable Energy for a Clean and Sustainable Future, Energy Sources 26 (2004) 1119–1129. https://doi.org/10.1080/00908310490441421.

[3] P. Moriarty, D. Honnery, Intermittent renewable energy: The only future source of hydrogen?, Int. J. Hydrog. Energy 32 (2007) 1616–1624. https://doi.org/10.1016/j.ijhydene.2006.12.008.

[4] P. Moriarty, D. Honnery, Can renewable energy power the future?, Energy Policy 93 (2016) 3–7. https://doi.org/10.1016/j.enpol.2016.02.051.

[5] A. Arregi, M. Amutio, G. Lopez, J. Bilbao, M. Olazar, Evaluation of thermochemical routes for hydrogen production from biomass: A review, Energy Convers. Manag. 165 (2018) 696–719. https://doi.org/10.1016/j.enconman.2018.03.089.

[6] P. Parthasarathy, K.S. Narayanan, Hydrogen production from steam gasification of biomass: Influence of process parameters on hydrogen yield – A review, Renew. Energy 66 (2014) 570–579. https://doi.org/10.1016/j.renene.2013.12.025.

[7] A.M. Parvez, S. Hafner, M. Hornberger, M. Schmid, G. Scheffknecht, Sorption enhanced gasification (SEG) of biomass for tailored syngas production with in-situ CO2 capture: Current status, process scale-up experiences and outlook, Renew. Sustain. Energy Rev. 141 (2021) 110756. https://doi.org/10.1016/j.rser.2021.110756.

[8] F. Dashtestani, M. Nusheh, V. Siriwongrungson, J. Hongrapipat, V. Materic, S. Pang, CO2 Capture from Biomass Gasification Producer Gas Using a Novel Calcium and Iron-Based Sorbent through Carbonation–Calcination Looping, Ind. Eng. Chem. Res. 59 (2020) 18447–18459. https://doi.org/10.1021/acs.iecr.0c03025.

[9] C. Pfeifer, B. Puchner, H. Hofbauer, In-Situ CO_2-Absorption in a Dual Fluidized Bed Biomass Steam Gasifier to Produce a Hydrogen Rich Syngas, Int. J. Chem. React. Eng. 5 (2007). https://doi.org/10.2202/1542-6580.1395.

[10] C. Dang, Y. Li, S.M. Yusuf, Y. Cao, H. Wang, H. Yu, F. Peng, F. Li, Calcium cobaltate: a phase-change catalyst for stable hydrogen production from bio-glycerol, Energy Environ. Sci. 11 (2018) 660–668. https://doi.org/10.1039/C7EE03301J.

[11] X. Zhao, H. Zhou, V.S. Sikarwar, M. Zhao, A.-H.A. Park, P.S. Fennell, L. Shen, L.-S. Fan, Biomass-based chemical looping technologies: the good, the bad and the future, Energy Environ. Sci. 10 (2017) 1885–1910. https://doi.org/10.1039/C6EE03718F.

[12] J. Wang, L. Huang, R. Yang, Z. Zhang, J. Wu, Y. Gao, Q. Wang, D. O'Hare, Z. Zhong, Recent advances in solid sorbents for CO_2 capture and new development trends, Energy Env. Sci 7 (2014) 3478–3518. https://doi.org/10.1039/C4EE01647E.

[13] M. Erans, V. Manovic, E.J. Anthony, Calcium looping sorbents for CO_2 capture, Appl. Energy 180 (2016) 722–742. https://doi.org/10.1016/j.apenergy.2016.07.074.

[14] M.T. Dunstan, A. Jain, W. Liu, S.P. Ong, T. Liu, J. Lee, K.A. Persson, S.A. Scott, J.S. Dennis, C.P. Grey, Large scale computational screening and experimental discovery of novel materials for high temperature CO_2 capture, Energy Environ. Sci. 9 (2016) 1346–1360. https://doi.org/10.1039/C5EE03253A.

[15] C.Y. Lau, M.T. Dunstan, W. Hu, C.P. Grey, S.A. Scott, Large scale in silico screening of materials for carbon capture through chemical looping, Energy Environ. Sci. 10 (2017) 818–831. https://doi.org/10.1039/C6EE02763F.

[16] M. Krödel, A. Landuyt, P.M. Abdala, C.R. Müller, Mechanistic Understanding of CaO-Based Sorbents for High-Temperature CO_2 Capture: Advanced Characterization and Prospects, ChemSusChem 13 (2020) 6259–6272. https://doi.org/10.1002/cssc.202002078.

[17] M.T. Dunstan, F. Donat, A.H. Bork, C.P. Grey, C.R. Müller, CO_2 Capture at Medium to High Temperature Using Solid Oxide-Based Sorbents: Fundamental Aspects, Mechanistic Insights, and Recent Advances, Chem. Rev. 121 (2021) 12681–12745. https://doi.org/10.1021/acs.chemrev.1c00100.

[18] S. Masoudi Soltani, A. Lahiri, H. Bahzad, P. Clough, M. Gorbounov, Y. Yan, Sorption-enhanced Steam Methane Reforming for Combined CO_2 Capture and Hydrogen Production: A State-of-the-Art Review, Carbon Capture Sci. Technol. 1 (2021) 100003. https://doi.org/10.1016/j.ccst.2021.100003.

[19] H. An, T. Song, L. Shen, C. Qin, J. Yin, B. Feng, Coal gasification with in situ CO_2 capture by the synthetic CaO sorbent in a 1 kWth dual fluidised-bed reactor, Int. J. Hydrog. Energy 37 (2012) 14195–14204. https://doi.org/10.1016/j.ijhydene.2012.06.077.

[20] A.S. Akdag, I. Durán, G. Gullu, C. Pevida, Performance of TSA and VSA post-combustion CO_2 capture processes with a biomass waste-based adsorbent, J. Environ. Chem. Eng. 10 (2022) 108759. https://doi.org/10.1016/j.jece.2022.108759.

[21] P.A. Webley, A. Qader, A. Ntiamoah, J. Ling, P. Xiao, Y. Zhai, A New Multi-bed Vacuum Swing Adsorption Cycle for CO_2 Capture from Flue Gas Streams, Energy Procedia 114 (2017) 2467–2480. https://doi.org/10.1016/j.egypro.2017.03.1398.

[22] B. Acharya, A. Dutta, P. Basu, Chemical-Looping Gasification of Biomass for Hydrogen-Enriched Gas Production with In-Process Carbon Dioxide Capture, Energy Fuels 23 (2009) 5077–5083. https://doi.org/10.1021/ef9003889.

[23] J. Udomsirichakorn, P. Basu, P. Abdul Salam, B. Acharya, CaO-based chemical looping gasification of biomass for hydrogen-enriched gas production with in situ CO_2 capture and tar reduction, Fuel Process. Technol. 127 (2014) 7–12. https://doi.org/10.1016/j.fuproc.2014.06.007.

[24] L. Brody, R. Cai, A. Thornton, J. Liu, H. Yu, F. Li, Perovskite-Based Phase Transition Sorbents for Sorption-Enhanced Oxidative Steam Reforming of Glycerol, ACS Sustain. Chem. Eng. 10 (2022) 6434–6445. https://doi.org/10.1021/acssuschemeng.2c01323.

[25] M. Ramezani, P. Tremain, E. Doroodchi, B. Moghtaderi, Determination of Carbonation/Calcination Reaction Kinetics of a Limestone Sorbent in low CO_2 Partial Pressures Using TGA Experiments, Energy Procedia 114 (2017) 259–270. https://doi.org/10.1016/j.egypro.2017.03.1168.

[26] A. Martínez, Lime enhanced biomass gasification. Energy penalty reduction by solids preheating in the calciner, Int. J. Hydrog. Energy 37 (2012) 15085–15095.

[27] M. Zhao, M. Bilton, A.P. Brown, A.M. Cunliffe, E. Dvininov, V. Dupont, T.P. Comyn, S.J. Milne, Durability of $CaO–CaZrO_3$ Sorbents for High-Temperature CO2 Capture Prepared by a Wet Chemical Method, Energy Fuels 28 (2014) 1275–1283. https://doi.org/10.1021/ef4020845.

[28] G. Gadikota, A.A. Park, Chapter 8 - Accelerated Carbonation of Ca- and Mg-Bearing Minerals and Industrial Wastes Using CO_2, in: P. Styring, E.A. Quadrelli, K. Armstrong

(Eds.), Carbon Dioxide Util., Elsevier, Amsterdam, 2015: pp. 115–137. https://doi.org/10.1016/B978-0-444-62746-9.00008-6.

[29] Z. Yang, M. Zhao, N.H. Florin, A.T. Harris, Synthesis and Characterization of CaO Nanopods for High Temperature CO_2 Capture, Ind. Eng. Chem. Res. 48 (2009) 10765–10770. https://doi.org/10.1021/ie901137s.

[30] M. Zhao, J. Shi, X. Zhong, S. Tian, J. Blamey, J. Jiang, P.S. Fennell, A novel calcium looping absorbent incorporated with polymorphic spacers for hydrogen production and CO_2 capture, Energy Env. Sci 7 (2014) 3291–3295. https://doi.org/10.1039/C4EE01281J.

[31] V. Manovic, P.S. Fennell, M.J. Al-Jeboori, E.J. Anthony, Steam-Enhanced Calcium Looping Cycles with Calcium Aluminate Pellets Doped with Bromides, Ind. Eng. Chem. Res. 52 (2013) 7677–7683. https://doi.org/10.1021/ie400197w.

[32] N. Phalak, W. Wang, L.-S. Fan, $Ca(OH)_2$-Based Calcium Looping Process Development at The Ohio State University, Chem. Eng. Technol. 36 (2013) 1451–1459. https://doi.org/10.1002/ceat.201200707.

[33] A.M. Kierzkowska, R. Pacciani, C.R. Müller, CaO-Based CO_2 Sorbents: From Fundamentals to the Development of New, Highly Effective Materials, ChemSusChem 6 (2013) 1130–1148. https://doi.org/10.1002/cssc.201300178.

[34] M. Krödel, A. Oing, J. Negele, A. Landuyt, A. Kierzkowska, A.H. Bork, F. Donat, C.R. Müller, Yolk–shell-type CaO-based sorbents for CO_2 capture: assessing the role of nanostructuring for the stabilization of the cyclic CO_2 uptake, Nanoscale 14 (2022) 16816–16828. https://doi.org/10.1039/D2NR04492G.

[35] M. Broda, A.M. Kierzkowska, C.R. Müller, Application of the Sol–Gel Technique to Develop Synthetic Calcium-Based Sorbents with Excellent Carbon Dioxide Capture Characteristics, ChemSusChem 5 (2012) 411–418. https://doi.org/10.1002/cssc.201100468.

[36] F.-C. Yu, N. Phalak, Z. Sun, L.-S. Fan, Activation Strategies for Calcium-Based Sorbents for CO2 Capture: A Perspective, Ind. Eng. Chem. Res. 51 (2012) 2133–2142. https://doi.org/10.1021/ie200802y.

[37] L.B. Braga, Hydrogen production by biogas steam reforming_ A technical, economic and ecological analysis, Renew. Sustain. Energy Rev. 28 (2013) 166–173.

[38] M. Krödel, C. Leroy, S.M. Kim, M.A. Naeem, A. Kierzkowska, Y.-H. Wu, A. Armutlulu, A. Fedorov, P. Florian, C.R. Müller, Of Glasses and Crystals: Mitigating the Deactivation

of CaO-Based CO_2 Sorbents through Calcium Aluminosilicates, JACS Au 3 (2023) 3111–3126. https://doi.org/10.1021/jacsau.3c00475.

[39] M. Krödel, L. Abduly, M. Nadjafi, A. Kierzkowska, A. Yakimov, A.H. Bork, F. Donat, C. Copéret, P.M. Abdala, C.R. Müller, Structure of Na Species in Promoted CaO-Based Sorbents and Their Effect on the Rate and Extent of the CO_2 Uptake, Adv. Funct. Mater. 33 (2023) 2302916. https://doi.org/10.1002/adfm.202302916.

[40] A. López-Ortiz, N.G.P. Rivera, A.R. Rojas, D.L. Gutierrez, Novel Carbon Dioxide Solid Acceptors Using Sodium Containing Oxides, Sep. Sci. Technol. 39 (2005) 3559–3572. https://doi.org/10.1081/SS-200036766.

[41] X. Yan, Y. Li, X. Ma, J. Zhao, Z. Wang, Performance of Li_4SiO_4 Material for CO_2 Capture: A Review, Int. J. Mol. Sci. 20 (2019) 928. https://doi.org/10.3390/ijms20040928.

[42] S. Jeoung, J.H. Lee, H.Y. Kim, H.R. Moon, Effects of porous carbon additives on the CO_2 absorption performance of lithium orthosilicate, Thermochim. Acta 637 (2016) 31–37. https://doi.org/10.1016/j.tca.2016.05.010.

[43] M.J. Venegas, E. Fregoso-Israel, R. Escamilla, H. Pfeiffer, Kinetic and Reaction Mechanism of CO_2 Sorption on Li_4SiO_4: Study of the Particle Size Effect, Ind. Eng. Chem. Res. 46 (2007) 2407–2412. https://doi.org/10.1021/ie061259e.

[44] L. Brody, M. Rukh, R. Cai, A.S. Bosari, R. Schomäcker, F. Li, Sorption-enhanced steam reforming of toluene using multifunctional perovskite phase transition sorbents in a chemical looping scheme, J. Phys. Energy 5 (2023) 035004. https://doi.org/10.1088/2515-7655/acdbe9.

[45] J. Hwang, R.R. Rao, L. Giordano, Y. Katayama, Y. Yu, Y. Shao-Horn, Perovskites in catalysis and electrocatalysis, Science 358 (2017) 751–756. https://doi.org/10.1126/science.aam7092.

[46] Y.S. Lin, Q. Yang, J. Ida, High temperature sorption of carbon dioxide on perovskite-type metal oxides, J. Taiwan Inst. Chem. Eng. 40 (2009) 276–280. https://doi.org/10.1016/j.jtice.2008.12.010.

[47] M.T. Dunstan, H. Laeverenz Schlogelhofer, J.M. Griffin, M.S. Dyer, M.W. Gaultois, C.Y. Lau, S.A. Scott, C.P. Grey, Ion Dynamics and CO $_2$ Absorption Properties of Nb-, Ta-, and Y-Doped Li $_2$ ZrO $_3$ Studied by Solid-State NMR, Thermogravimetry, and First-Principles

Calculations, J. Phys. Chem. C 121 (2017) 21877–21886. https://doi.org/10.1021/acs.jpcc.7b05888.

[48] M.T. Dunstan, J.M. Griffin, F. Blanc, M. Leskes, C.P. Grey, Ion Dynamics in Li_2CO_3 Studied by Solid-State NMR and First-Principles Calculations, J. Phys. Chem. C 119 (2015) 24255–24264. https://doi.org/10.1021/acs.jpcc.5b06647.

[49] Y. Zeng, N.J. Szymanski, T. He, K. Jun, L.C. Gallington, H. Huo, C.J. Bartel, B. Ouyang, G. Ceder, Selective formation of metastable polymorphs in solid-state synthesis, Sci. Adv. 10 (2024) eadj5431. https://doi.org/10.1126/sciadv.adj5431.

[50] A. Miura, C.J. Bartel, Y. Goto, Y. Mizuguchi, C. Moriyoshi, Y. Kuroiwa, Y. Wang, T. Yaguchi, M. Shirai, M. Nagao, N.C. Rosero-Navarro, K. Tadanaga, G. Ceder, W. Sun, Observing and Modeling the Sequential Pairwise Reactions that Drive Solid-State Ceramic Synthesis, Adv. Mater. 33 (2021) 2100312. https://doi.org/10.1002/adma.202100312.

[51] K.S. Sultana, D.T. Tran, J.C. Walmsley, M. Rønning, D. Chen, CaO Nanoparticles Coated by ZrO_2 Layers for Enhanced CO_2 Capture Stability, Ind. Eng. Chem. Res. 54 (2015) 8929–8939. https://doi.org/10.1021/acs.iecr.5b00423.

[52] J. Yin, C. Qin, B. Feng, L. Ge, C. Luo, W. Liu, H. An, Calcium Looping for CO_2 Capture at a Constant High Temperature, Energy Fuels 28 (2014) 307–318. https://doi.org/10.1021/ef401399c.

[53] Y.A. Criado, B. Arias, J.C. Abanades, Effect of the Carbonation Temperature on the CO_2 Carrying Capacity of CaO, Ind. Eng. Chem. Res. 57 (2018) 12595–12599. https://doi.org/10.1021/acs.iecr.8b02111.

[54] F. Donat, N.H. Florin, E.J. Anthony, P.S. Fennell, Influence of High-Temperature Steam on the Reactivity of CaO Sorbent for CO2 Capture, Environ. Sci. Technol. 46 (2012) 1262–1269. https://doi.org/10.1021/es202679w.

[55] A.D. Lalsare, High Pressure Steam Reactivation of Calcium Oxide Sorbents For Carbon Dioxide Capture Using Calcium Looping Process, The Ohio State University, 2016. https://etd.ohiolink.edu/apexprod/rws_olink/r/1501/10?clear=10&p10_accession_num=osu1462444410 (accessed July 4, 2023).

[56] W. Luo, A. Asthagiri, An ab initio thermodynamics study of cobalt surface phases under ethanol steam reforming conditions, Catal Sci Technol 4 (2014) 3379–3389. https://doi.org/10.1039/C4CY00582A.

[57] E.J. Popczun, T. Jia, S. Natesakhawat, C.M. Marin, T. Nguyen-Phan, Y. Duan, J.W. Lekse, Investigation of $Sr_{0.7}Ca_{0.3}FeO_3$ Oxygen Carriers with Variable Cobalt B-Site Substitution, ChemSusChem 14 (2021) 1893–1901. https://doi.org/10.1002/cssc.202002849.